Acta Cryst B
STRUCTURAL SCIENCE
CRYSTAL ENGINEERING
MATERIALS

ISSN 2052-5206

Received 27 February 2017
Accepted 2 June 2017

Edited by J. Benedict, University of Washington, USA

Keywords: charge and spin densities; X-ray and polarized neutron diffraction; joint refinement; DFT and CASSCF calculations; nitronyl nitroxide free radical.

CCDC reference: 1553900

Supporting information: this article has supporting information at journals.iucr.org/b

When combined X-ray and polarized neutron diffraction data challenge high-level calculations: spin-resolved electron density of an organic radical

Ariste Bolivard Voufack,[a,b] Nicolas Claiser,[a,b] Claude Lecomte,[a,b] Sébastien Pillet,[a,b] Yves Pontillon,[c] Béatrice Gillon,[d] Zeyin Yan,[e] Jean-Michel Gillet,[e] Marco Marazzi,[f,g] Alessandro Genoni[f,g] and Mohamed Souhassou[a,b]*

[a]Université de Lorraine, Laboratoire CRM2, UMR CNRS 7036, Boulevard des aiguillettes BP70239, 54506 Vandoeure-les-Nancy, France, [b]CNRS, Laboratoire CRM2, UMR CNRS 7036, Boulevard des aiguillettes BP70239, 54506 Vandoeure-les-Nancy, France, [c]DEN/CAD/DEC/SA3C/LAMIR, CEA Cadarache CEDEX, 13108 St Paul lez Durance, France, [d]LLB, CEA-CNRS, UMR 12, CEA Saclay, 91191 Gif-sur-Yvette CEDEX, France, [e]SPMS, UMR 8580, CentraleSupelec, Grande Voie des Vignes, 92295 Chatenay-Malabry CEDEX, France, [f]Université de Lorraine, Laboratoire SRSMC, UMR CNRS 7565, Boulevard des Aiguillettes BP 70239, 54506Vandoeuvre-lès-Nancy CEDEX, France, and [g]CNRS, Laboratoire SRSMC, UMR 7565, Boulevard des Aiguillettes BP 70239, 54506 Vandoeuvre-lès-Nancy CEDEX, France. *Correspondence e-mail: mohamed.souhassou@univ-lorraine.fr

Joint refinement of X-ray and polarized neutron diffraction data has been carried out in order to determine charge and spin density distributions simultaneously in the nitronyl nitroxide (NN) free radical Nit(SMe)Ph. For comparison purposes, density functional theory (DFT) and complete active-space self-consistent field (CASSCF) theoretical calculations were also performed. Experimentally derived charge and spin densities show significant differences between the two NO groups of the NN function that are not observed from DFT theoretical calculations. On the contrary, CASSCF calculations exhibit the same fine details as observed in spin-resolved joint refinement and a clear asymmetry between the two NO groups.

1. Introduction

Based on the pioneering work of Becker & Coppens (1985), we have recently described a new method for modelling spin-resolved electron distributions in crystals from combined X-ray (XRD), unpolarized (ND) and polarized neutron (PND) diffraction data (Deutsch *et al.*, 2014). Accurate XRD data allow for the reconstruction of the total electron density $\rho(\mathbf{r})$, while PND provides necessary information to recover the spin density $s(\mathbf{r})$. These two quantities are, respectively, the sum and the difference of spin up and spin down electron distributions.

$$\rho(\mathbf{r}) = \rho_{\uparrow}(\mathbf{r}) + \rho_{\downarrow}(\mathbf{r}) \qquad s(\mathbf{r}) = \rho_{\uparrow}(\mathbf{r}) - \rho_{\downarrow}(\mathbf{r}) \tag{1}$$

Spin-resolved electron distributions are analyzed with the 'spin split multipolar atom model' simultaneously refined against XRD, PND and ND data. More precisely, the electron density distribution is modelled using a generalized Hansen Coppens (HC) model (Hansen & Coppens, 1978) in a joint refinement procedure as developed in the *Mollynx* program (Deutsch *et al.*, 2012). The total density is expressed as the sum of pseudo-atomic contributions, where the density associated with an atomic centre i is

$$\begin{aligned}\rho_i(\mathbf{r}) = {} & \rho_i^{(\mathrm{core})}(r) + P_i^{\uparrow(\mathrm{val})}\kappa_i^{\uparrow 3}\rho_i^{(\mathrm{val})}\left(\kappa_i^{\uparrow} r\right) + P_i^{\downarrow(\mathrm{val})}\kappa_i^{\downarrow 3}\rho_i^{(\mathrm{val})}\left(\kappa_i^{\downarrow} r\right) \\ & + \sum_{\ell}\kappa_i'^{\uparrow 3}R_{i,\ell}^{(\mathrm{val})}\left(\kappa_i'^{\uparrow} r\right)\sum_{m=0}^{\ell}P_{i,\ell,m\pm}^{\uparrow}y_{\ell,m\pm}(\theta,\varphi) \\ & + \sum_{\ell}\kappa_i'^{\downarrow 3}R_{i,\ell}^{(\mathrm{val})}\left(\kappa_i'^{\downarrow} r\right)\sum_{m=0}^{\ell}P_{i,\ell,m\pm}^{\downarrow}y_{\ell,m\pm}(\theta,\varphi),\end{aligned} \tag{2}$$

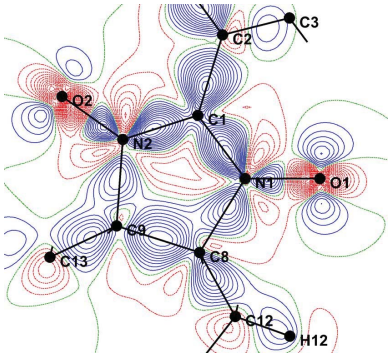

where $P^{\uparrow(\mathrm{val})}$, $P^{\uparrow}_{\ell,m}$, $P^{\downarrow(\mathrm{val})}$ and $P^{\downarrow}_{\ell,m}$ refer to spin up and spin down refined population parameters, respectively, $\kappa^{\uparrow}$ and $\kappa^{\downarrow}$ are the refined expansion contraction parameters. Such formalism has been successfully tested (Deutsch *et al.*, 2014) on a Cu_2 molecular magnet showing the drastic difference between spin up and spin down angular distributions around the Cu atoms, in excellent agreement with *ab initio* calculations carried out at the DFT level. In this paper we apply this formalism to a pure organic free radical crystal for the first time. The quality of experimental data and fine modelling of the density using the joint refinement opens up a high level of accuracy so that it can be employed to challenge very sophisticated *ab initio* techniques of theoretical chemistry.

This study has been carried out on 2-(4-thiomethylphenyl)-4,4,5,5-tetramethylimidazoline-1-oxyl-3-oxide [Nit(SMe)Ph], which belongs to the nitronyl-nitroxide free radical family, extensively studied since the discovery of the first purely organic ferromagnet, *p*-nitrophenyl nitronyl nitroxide (*p*-NPNN; Nakazawa *et al.*, 1992). Nitronyl nitroxide is a stable free radical and carries a delocalized unpaired electron (S = 1/2) over two NO groups. It is the most widely used radical in the design of molecular magnets because it can propagate magnetic interactions from one molecule to another in crystalline solids when the packing is adequately tuned. Hydrogen bonding can further control the crystalline molecular arrangement, and therefore direct-through-space magnetic coupling in the crystal, leading in some cases to ferromagnetic ordering (Zhang *et al.*, 2006; Sugawara *et al.*, 1994). In polymetallic systems, the NO group may be used as a linker between metal ions to enhance the spin ground state (Caneschi *et al.*, 1989; Kahn *et al.*, 2000; Zhu *et al.*, 2014; Woodruff *et al.*, 2013; Wang *et al.*, 2016). Such NN-based polymetallic molecular magnetic materials with different types of spin centres (*p–d*, *p–f*, *p–d–f*) led to new developments of single molecule or single chain magnets with potentially high T_C/T_B (see, for example, Harriman & Murugesu, 2016).

Magnetic ordering in crystalline molecular materials is related to the spatial arrangement of the molecular short contacts between spin carriers (Novoa *et al.*, 2011, and reference therein) and especially to the hydrogen-bonding patterns. To assess the importance of intermolecular interactions on magnetic coupling in organic ferromagnets, experimental joint refinement and two different types of theoretical calculation (DFT and CASSCF) were carried out on the prototype compound Nit(SMe)Ph.

2. Methodology

2.1. Experiment and joint refinement

Nit(SMe)Ph (Fig. 1) is a radical in which an unpaired electron is mainly described by the π^* SOMO orbital (singly occupied molecular orbital), which is a linear combination of orbitals (mainly $2p_z$) centered on the O2, N2, C1, N1 and O1 atoms. Nit(SMe)Ph crystallizes in monoclinic space group $P2_1/a$, with a = 9.340 (2), b = 19.482 (4), c = 8.634 (1) Å and β = 115.13 (1)°

This radical behaves as a paramagnetic S = 1/2 unit and undergoes ferromagnetic ordering at very low temperature (T_C = 0.2 K) (Caneschi, Ferraro, Gateschi, Le Lirzin, Novak *et al.*, 1995; Caneschi, Ferraro, Gateschi, Le Lirzin & Rentschler, 1995). Nit(SMe)Ph was also studied using polarized neutron diffraction (Pontillon *et al.*, 1999). From these studies, an intermolecular charge transfer mechanism was proposed where the unpaired electron is transferred from the SOMO to the LUMO (lowest unoccupied molecular orbital) molecular orbital. The SOMO is localized on the ONCNO group and the LUMO extends from the thio-methyl group to the NO functions. This mechanism is believed to be assisted by hydrogen bonds leading to magnetic ordering at low temperature. The previous analysis of experimental charge density (Pillet *et al.*, 2001) was in line with this mechanism. In order to acquire deeper insight into the magnetic interaction mechanism, it was decided to further explore this compound by simultaneously modelling spin and charge density distributions using the XRD and PND published data through a joint refinement process.

The total electron density has been initially modelled with the usual HC model and the resulting position, thermal and electron density parameters were the starting values of the following joint refinement. Modelling the spin electron distribution requires selecting the magnetic atoms for which electron populations will be split into up and down contributions. The O2—N2—C1—N1—O1 atoms of the NN function (see Fig. 1) are expected to bear most of the electron-magnetic contribution. Therefore, the electron populations of these five atoms were split into up and down [equation (2)] and refined independently. Since potential pathways for exchange interaction between radicals are hydrogen bonds (HB), and since there is a delocalized π-orbital which extends from the C5—S bond to C1—N1 and C1—N2 bonds, all the valence monopoles P^{val} for the atoms of the molecular skeleton were split. As only the atoms of the O—N—C—N—O group carry a significant magnetic moment, their multipole parameters [$P_{lm} > 5\sigma(P_{lm})$] were refined up to quadrupole level. Experimental

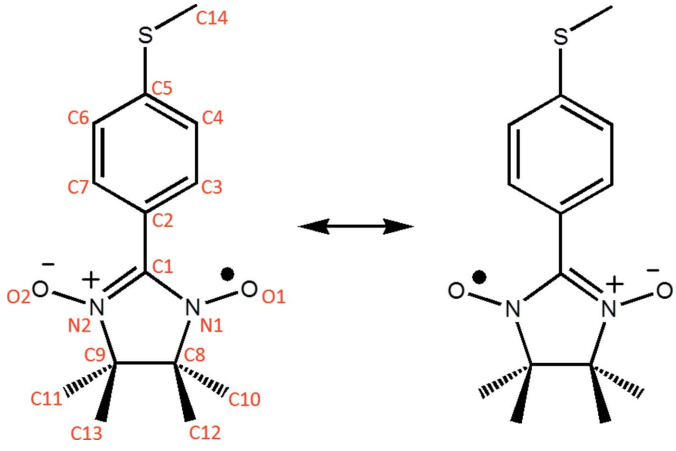

Figure 1
Main resonance structures of Nit(SMe)Ph. On the left one, the labels of the main atoms are reported, while H atoms are omitted for the sake of clarity.

Table 1
Statistical agreement factors after joint refinement.

Indices X and PN refer to X-ray and polarized neutron, *N*ref are the corresponding number of reflections.

R_X	wR_X	GoF_X	$Nref_X$	R_{PN}	wR_{PN}	GoF_{PN}	$Nref_{PN}$	
0.020	0.026	0.917	8800	–	–	–	–	X rays only
0.019	0.025	0.880	8800	0.073	0.006	1.675	352	Joint refinement

conditions and statistical agreements are given in Table 1. The very good agreement indices together with almost featureless residual electron density maps (Fig. 2) show the high quality of the model and its adequacy to thoroughly account for most of the physical information contained in the experimental data.

The resulting charge and spin density distributions are in agreement with our previous studies. The positive spin density is mainly distributed on the N and O atoms while C1 bears negative spin density. Following the joint refinement, the static deformation density of the NN ring (see Fig. 3*a*) is in excellent agreement with that previously obtained (Pillet *et al.*, 2001). Both static charge and spin density maps reveal significant differences between the two N—O groups. Such an asymmetry is also visible on the spin-resolved electron densities, spin up and spin down electron density maps (Figs. S1 and S2 of the supporting information).

The asymmetries are due to slight differences in the refined charge and spin density parameters of the two NO groups which were treated independently in the joint refinement. In addition and most importantly, this leads to differences in the integrated spin populations over the atomic basins (called hereafter Bader spin populations; see Table 2 and Table 3), which are uniquely defined in Bader's partitioning of space (quantum theory of atoms in molecules, QTAIM; Bader, 1990).

2.2. Computational methods

To acquire more insight into these differences, theoretical calculations were carried out in order to identify the origin of the experimentally observed asymmetry. For that purpose, calculations were performed for an isolated radical and for a dimer of radicals linked through hydrogen bonds, to probe the influence of intermolecular interactions and crystal packing. Two types of *ab initio* methods have been considered as particularly well adapted for our purpose: density functional theory (DFT; Parr & Yang, 1989; Perdew *et al.*, 2009; Jones, 2015) and multi-configurational CASSCF (complete active-space self-consistent field; Roos, 1987).

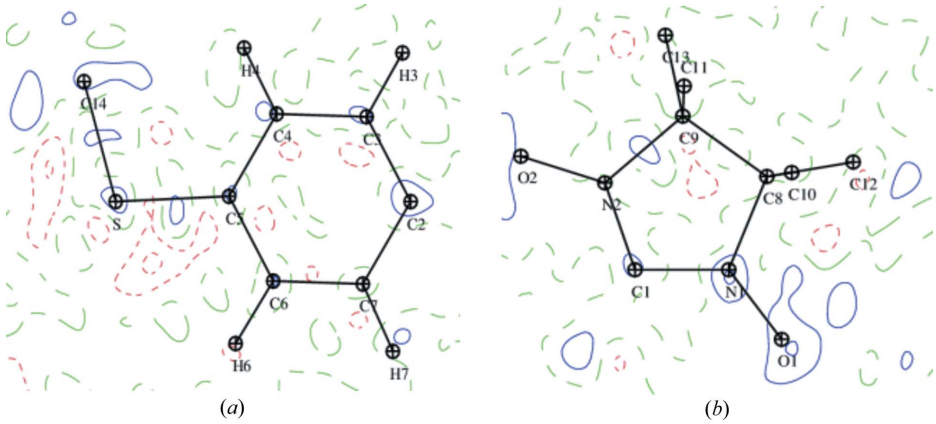

(*a*) (*b*)

Figure 2
Residual electron density maps in the phenyl ring plane (*a*) and Nit ring (*b*) plane. Contour intervals of 0.05 e Å^{-3}, positive (blue), negative (red) and neutral (green) lines.

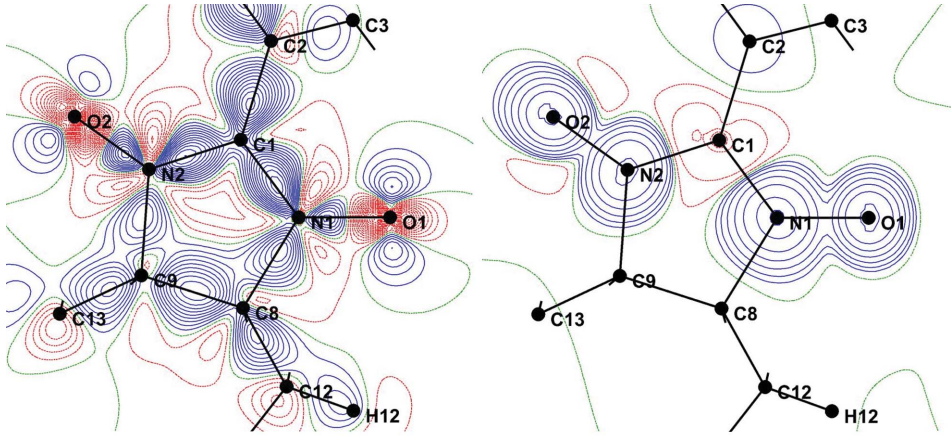

(*a*) (*b*)

Figure 3
Experimental static deformation electron density (*a*, contour intervals of 0.05 e Å^{-3}) and spin density (*b*, contour intervals of 0.01 × 2^n (n = 0, ...,12) μ_B Å^{-3}) in the plane of two NO groups [positive (blue) negative (red) and neutral (green)].

Table 2
Spin populations (in μ_B) obtained from the joint refinement ($\Delta P_i^{val} = P_i^{val\uparrow} - P_i^{val\downarrow}$) and from DFT/M06-2X and CASSCF (7, 8) calculations (cc-pVDZ basis-set) performed on the monomer.

No error bars on the Bader populations are provided by the Bader analysis of the experimental spin density.

	ΔP^{val}	Mulliken populations		Bader populations		
Atom	Joint refinement	M06-2X	CASSCF	Joint refinement	M06-2X	CASSCF
O1	0.24 (1)	0.37	0.30	0.27	0.35	0.29
N1	0.33 (1)	0.28	0.30	0.27	0.26	0.28
C1	−0.15 (2)	−0.27	−0.17	−0.08	−0.19	−0.12
N2	0.29 (1)	0.27	0.27	0.25	0.25	0.25
O2	0.21 (1)	0.36	0.29	0.23	0.34	0.28
N1+O1	0.56 (2)	0.66	0.60	0.54	0.62	0.57
N2+O2	0.50 (2)	0.63	0.56	0.48	0.60	0.54

All the *ab initio* computations were performed using the experimental geometry of the radical (as a monomer or a dimer) as determined from the joint refinement. Therefore, no geometry optimization was conducted in order to preserve all the observed intra- and inter-molecular interactions in the X-ray and polarized neutron diffraction experiments. The chosen dimer is made of two radicals linked by the two shortest intermolecular hydrogen bonds observed in the crystal structure (Fig. 5; O1—H141: 2.515 Å and O2—H103: 2.333 Å). The two molecules are related by a glide mirror symmetry operation (perpendicular to the *b* axis).

In particular, the DFT computations were carried out through the *GAUSSIAN*09 package (Frisch *et al.*, 2009) using the M06-2X (Zhao & Truhlar, 2008), CAM-B3LYP (Takeshi *et al.*, 2004) and B3LYP (Becke, 1993) hybrid functionals coupled with the standard basis-set cc-pVDZ. The CASSCF calculations were performed by means of the MOLCAS code (Aquilante *et al.*, 2016), always with the standard basis-set cc-pVDZ and using the (7,8) and (10,10) active spaces for the monomer and dimer, respectively (see supporting information for details about the choice of the active spaces, Tables S1 and S2).

Table 3
Bader spin populations (in μ_B) obtained from DFT/M06-2X and CASSCF (10, 10) calculations (cc-pVDZ basis-set) performed on the Nit(SMe)Ph dimer.

	M06-2X		CASSCF	
Atom	Dimer (mol 1)	Dimer (mol 2)	Dimer (mol 1)	Dimer (mol 2)
O1	0.36	0.34	0.32	0.29
N1	0.27	0.27	0.28	0.29
C1	−0.18	−0.18	−0.12	−0.12
N2	0.26	0.26	0.28	0.29
O2	0.33	0.33	0.23	0.23
N1+O1	0.62	0.61	0.58	0.60
N2+O2	0.59	0.59	0.52	0.50

In particular, an exhaustive spin population analysis was performed in order to compare the obtained theoretical values with the experimental results. Preliminary estimates based on the Mulliken approximation, which is known to significantly depend on the adopted basis-set, were carried out in order to provide a qualitative comparison with the experimentally refined $P_i^{\uparrow}$ and $P_i^{\downarrow}$ parameters of the spin split model. Then a more rigorous, and less biased, analysis was performed to evaluate theoretical spin populations by integration of the spin densities over the QTAIM atomic basins obtained from the topological analysis of the electron distribution.

For the sake of clarity, in this paper we will only report the results (see Tables 2 and 3) obtained at CASSCF and unrestricted-M06-2X levels on the Nit(SMe)Ph monomer and dimer. All the other unrestricted and restricted open-shell DFT results are shown for the sake of completeness in the supporting information (see Tables S3 and S4).

3. Discussion and conclusions

Several conclusions can be drawn from these results. Considering that spin density only arises from the contribution of a single electron per molecule (out of the 149 electrons involved in the scattering process and in the theoretical calculations), the overall agreement of experimental reconstruction with *ab initio* calculated spin densities is quite remarkable. Such an

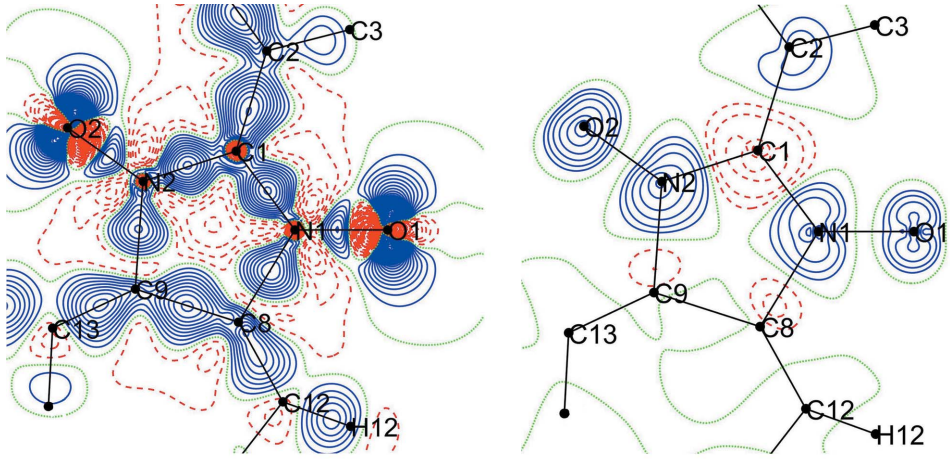

(*a*) (*b*)

Figure 4
Static deformation (*a*) and spin density (*b*) maps (as in Figs. 3*a* and *b*) from DFT calculations on the monomer.

unprecedented experimental accuracy can be reached because PND results are interpreted in conjunction with high-resolution XRD data which allow the use of a more sophisticated model (the spin-split model), with highly relevant chemical parameters. Furthermore, the observed experimental spin density (as well as the charge density) exhibits a marked asymmetry between both nitroxide groups (see spin population and charge distribution), which is not reproduced at the DFT level on the monomer (Fig. 4; Table 2) and the dimer (Table 3), where the differences between monomer and dimer are marginal. However, this asymmetry is observed in CASSCF calculations on the monomer and is slightly enhanced on the dimer. It is thus a sign of high experimental reliability to observe that the difference in spin density distribution can only be reproduced when a CASSCF calculation is performed. In fact, due to its particular multi-determinant nature, the CASSCF technique is intrinsically able to describe the multi-reference character of the system in exam, thus being able to assign a different weight to the resonance structures depicted in Fig. 1. This very subtle difference, at the precision limit, could have been interpreted as an experimental artefact, but it actually proves to be a new challenge for theoretical methods. Furthermore, the Bader populations obtained starting from the CASSCF calculation performed on the dimer show an even increased discrepancy between the spin populations of the two nitroxide groups (see Table 2), thus indicating that the experimentally observed asymmetry has probably both an intra- and inter-molecular origin. This asymmetry was also observed in a similar compound ((Zhang *et al.*, 2006) and was attributed to hydrogen bonding and hyperconjugation over the phenyl ring.

Finally, the distribution of spin density on N and O atoms in each nitroxide group has been quite controversial for several decades. While standard first-principle calculations, at the (unrestricted) Hartree–Fock or DFT levels tend to attribute a significantly stronger contribution to the oxygen sites (for example, Gillon *et al.*, 1983; Delley *et al.*, 1984; Improta *et al.*, 2002; Barone *et al.*, 2009), analysis from PND consistently showed that the distribution was more evenly distributed between both atoms and sometimes the spin on the nitrogen sites is even more significant than on the oxygen sites (Brown *et al.*, 1983; Bordeaux *et al.*, 1993; Pontillon *et al.*, 1999. Here again, the CASSCF calculations of this work tend to confirm this early experimental prediction by attributing an almost equal spin population to the oxygen and nitrogen atomic basins.

In order to understand the origin of the differences between the two N—O groups in the monomer, extended CASSCF calculations are being performed as a function of the dihedral angle between the phenyl group and the nitronyl nitroxide ring to evaluate the intramolecular contribution and will be discussed in a future publication.

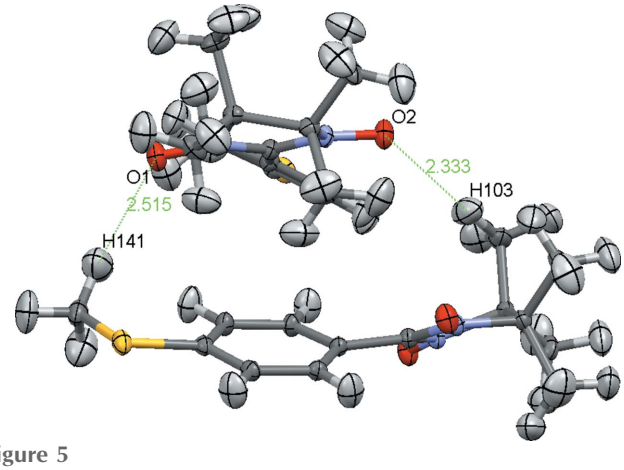

Figure 5
ORTEP view of the dimer used for theoretical calculation.

Funding information

The following funding is acknowledged: Agence Nationale de la Recherche (award No. ANR-MTMED2014).

References

Aquilante, F. *et al.* (2016). *J. Comput. Chem.* **37**, 506–541.
Bader, R. F. W. (1990). *Atoms in Molecules: A Quantum Theory.* Oxford University Press.
Barone, V., Cacelli, I. & Ferretti, A. (2009). *J. Chem. Phys.* **130**, 094306.
Becke, A. D. (1993). *J. Chem. Phys.* **98**, 1372–1377.
Becker, P. & Coppens, P. (1985). *Acta Cryst.* A**41**, 177–182.
Bordeaux, D., Boucherle, J. X., Delley, B., Gillon, B., Ressouche, E. & Schweizer, J. (1993). *Z. Naturforsch. A*, **48**, 117–119.
Brown, P. J., Capiomont, A., Gillon, B. & Schweizer, J. (1983). *Mol. Phys.* **48**, 753–761.
Caneschi, A., Ferraro, F., Gatteschi, D., Le Lirzin, A., Novak, M., Rentschler, E. & Sessoli, R. (1995). *Adv. Mater.* **7**, 476–478.
Caneschi, A., Ferraro, F., Gatteschi, D., Le Lirzin, A. & Rentschler, E. (1995). *Inorg. Chem. Acta*, **235**, 159.
Caneschi, A., Gatteschi, D., Sessoli, R. & Rey, P. (1989). *Acc. Chem. Res.* **22**, 392–398.
Delley, B., Becker, P. & Gillon, B. (1984). *J. Chem. Phys.* **80**, 4286–4289.
Deutsch, M., Claiser, N., Pillet, S., Chumakov, Y., Becker, P., Gillet, J.-M., Gillon, B., Lecomte, C. & Souhassou, M. (2012). *Acta Cryst.* A**68**, 675–686.
Deutsch, M., Gillon, B., Claiser, N., Gillet, J.-M., Lecomte, C. & Souhassou, M. (2014). *IUCrJ*, **1**, 194–199.
Frisch, M. J. *et al.* (2009). *GAUSSIAN09*, Revisions D. 01. Gaussian, Inc., Wallingford, CT, USA.
Gillon, B., Becker, P. & Ellinger, Y. (1983). *Mol. Phys.* **48**, 763–774.
Hansen, N. K. & Coppens, P. (1978). *Acta Cryst.* A**34**, 909–921.
Harriman, K. L. & Murugesu, M. (2016). *Acc. Chem. Res.* **49**, 1158–1167
Improta, R., Kudin, K. N., Scuseria, G. E. & Barone, V. (2002). *J. Am. Chem. Soc.* **124**, 113.
Jones, R. O. (2015). *Rev. Mod. Phys.* **87**, 897–923.
Kahn, M. L., Sutter, J.-P., Golhen, S., Guionneau, P., Ouahab, L., Kahn, O. & Chasseau, D. (2000). *J. Am. Chem. Soc.* **122**, 3413–3421.
Nakazawa, Y., Tamura, M., Shirakawa, N., Shiomi, D., Takahashi, M. M., Kinoshita, M. & Ishikawa, M. (1992). *Phys. Rev. B*, **46**, 8906–8914.
Novoa, J. J., Deumal, M. & Jornet-Somoza, J. (2011). *Chem. Soc. Rev.* **40**, 3182–3212.
Parr, R. G. & Yang, W. (1989). *Density-Functional Theory of Atoms and Molecules.* Oxford University Press.
Perdew, J. P. A. R., Ruzsinszky, A., Constantin, L. A., Sun, J. & Csonka, G. I. (2009). *J. Chem. Theory Comput.* **5**, 902–908.

Pillet, S., Souhassou, M., Pontillon, Y., Caneschi, A. D. G., Gatteschi, D. & Lecomte, C. (2001). *New J. Chem.* **25**, 131–143.
Pontillon, Y., Akita, T., Grand, A., Kobayashi, K., Lelievre-Berna, E., Pécaut, J., Ressouche, E. & Schweizer, J. (1999). *J. Am. Chem. Soc.* **121**, 10126–10133.
Pontillon, Y., Caneschi, A., Gatteschi, D., Grand, A., Ressouche, E. S. R. & Schweizer, J. (1999). *Chem. Eur. J.* **5**, 3616–3624.
Pontillon, Y., Caneschi, A., Gatteschi, D., Ressouche, E., Schweizer, J. & Sessoli, R. (1999). *Physica B*, **267–268**, 51–55.
Roos, B. O. K. (1987). *Advanced Chemistry and Physics: Ab Initio Methods in Quantum Chemistry II*, edited by K. P. Lawley. Chicester, UK: Wiley.
Sugawara, T., Matsushita, M. M., Izuoka, A., Wada, N., Takeda, N. & Ishikawa, M. (1994). *J. Chem. Soc. Chem. Commun.* pp. 1723–1724.
Takeshi, Y., Tew, D. P. & Handy, N. C. (2004). *Chem. Phys. Lett.* **393**, 51–57.
Wang, J., Li, J.-N., Zhang, S.-L., Zhao, X., Shao, D. & Wang, X. (2016). *Chem. Commun.* **52**, 5033–5036.
Woodruff, D. N., Winpenny, R. E. P. & Layfield, R. A. (2013). *Chem. Rev.* **113**, 5110–5148.
Zhang, Y. S., Yao, K. L., Liu, Z. L., Yu, L. H. & Wang, X. L. (2006). *J. Chem. Phys.* **124**, 144712.
Zhao, Y. & Truhlar, D. J. (2008). *Theor. Chem. Acc.* **120**, 215–241.
Zhu, M., Mei, X.-L., Ma, Y., Li, L.-C., Liao, D.-Z. & Sutter, J.-P. (2014). *Chem. Commun.* **50**, 1906–1908.